Combined EXAFS and first-principles theory study of $Pb_{1-x}Ge_xTe$

B. Ravel and E. Cockayne
National Institute of Standards and Technology, Gaithersburg, Maryland 20899

M. Newville
Consortium for Advanced Radiation Sources, The University of Chicago, Chicago, Illinois 60637

K. M. Rabe
Department of Applied Physics, Yale University, New Haven, Connecticut 06520

(Received 28 May 1999)

The narrow band-gap semiconductor $Pb_{1-x}Ge_xTe$ has a low-temperature ferroelectric rhombohedral phase whose average structure is a distorted rocksalt structure. We have measured the extended x-ray-absorption-fine-structure (EXAFS) spectra of $Pb_{1-x}Ge_xTe$ with $x \approx 0.3$ at the Ge and Te K edges and at the Pb L_{III} edge. Guided by first-principles calculations, we create a model for the local structure as a distortion from the ideal rocksalt structure. By corefining the spectra from these three edges, we demonstrate that the data are consistent with our fitting model and we directly measure several secondary structural distortions predicted by the theory. This work demonstrates a powerful approach to the determination of local structures in complex materials by using first-principles calculations in conjunction with EXAFS measurements. [S0163-1829(99)13041-8]

Ferroelectric solid solutions are of theoretical and experimental interest as well as of significant technological importance. The macroscopic properties of ferroelectric solid solutions are strongly dependent not only on the average crystal structure, but on the details of the short-range atomic arrangements. Recent advances both in extended x-ray-absorption-fine-structure (EXAFS) spectroscopy and in first-principles calculations allow highly detailed computation and measurement of local structures in ferroelectric materials. $Pb_{1-x}Ge_xTe$ is a good prototype for these studies as the structure and physics of the ferroelectric phase are relatively simple and are known to be dominated by the off-center displacements of Ge ions with respect to their near-neighbor Te octahedra.[1]

In this work, we address this problem by combining recent advances in EXAFS spectroscopy with theoretical first-principles local-density-functional theory (LDFT) calculations to determine the local structure of the ferroelectric narrow-gap semiconductor $Pb_{1-x}Ge_xTe$. The average structure of the paraelectric high-temperature phase in $Pb_{1-x}Ge_xTe$ is rocksalt as shown in Fig. 1. For $x > 0.005$, the low-temperature phase is ferroelectric, with a rhombohedral unit cell only slightly distorted from cubic ($\alpha \approx 90°$). A class of simple phenomenological models for the paraelectric-ferroelectric transition in $Pb_{1-x}Ge_xTe$ is based on Ge off-center displacements.[1] In these models, individual Ge ions become more stable by moving from their nominal lattice positions in one of the eight cubic $\langle 111 \rangle$ directions. Below the transition temperature T_c, there is long-range order in the *direction* of off-center displacement of the Ge ions, resulting in a nonzero spontaneous polarization. Above T_c, there is no long-range order in the direction of the off-centering, and thus the material is paraelectric. Previous EXAFS work[1] revealed large displacements of the Ge ions both below and above the rhombohedral-to-cubic phase transition, supporting this phenomenological viewpoint.

$Pb_{1-x}Ge_xTe$ is a solid solution in which the configuration of the Pb and Ge cations is disordered. Nonetheless, it is formally possible to describe the ground-state ionic coordinates for any arbitrary configuration via a cluster expansion. In a cluster expansion, the Cartesian coordinate $u_{i,\alpha}$ for ion i of species S_i relative to its nominal rocksalt coordinate $u_{i,\alpha 0}$ is expanded in terms of the cation configuration

$$u_{i,\alpha} = u_{i,\alpha 0} + u_{S_i,\alpha} + \sum_j J_{S_i,\alpha(\mathbf{r}_j - \mathbf{r}_i)} \sigma_j + \sum_j \sum_k K_{S_i,\alpha(\mathbf{r}_j - \mathbf{r}_i, \mathbf{r}_k - \mathbf{r}_i)} \sigma_j \sigma_k + \text{higher order terms}, \tag{1}$$

where the indices j and k run over all cations, $u_{S,\alpha}$ is the coordinate in the α Cartesian direction for species S in the limit that all cations are Pb (i.e., with no Ge substitution), J and K are the linear and quadratic parameters in the cluster expansion, and σ_j is a coordinate describing the identity of cation j. Since we are interested in Pb-rich $Pb_{1-x}Ge_xTe$, we choose $\sigma = 0$ for Pb and $\sigma = 1$ for Ge. In order to obtain a

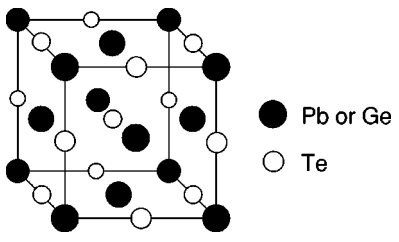

FIG. 1. The cubic rocksalt structure forms the basis of the local structure of $Pb_{1-x}Ge_xTe$. In the real material, the Ge ions randomly populate the sites indicated by black circles. In the LDFT calculations, these sites are populated by Ge ions in an ordered manner as shown in Ref. 4.

unique set of parameters, it is necessary to specify the orientation of each configuration. We choose a convention whereby the pseudocubic axes of a given configuration deviate from the Cartesian axes by a small irrotational strain and the orientation of its polarization vector is in the [111] quadrant.

Our primary goal in this work is to provide a more detailed description of the local structure in the ferroelectric phase of $Pb_{1-x}Ge_xTe$, based on Eq. (1). We exploit advances in theoretical and analytical tools developed in the years since the earlier EXAFS work to provide a more complete picture of the local structure of this material, including secondary distortions not considered in earlier models. Our secondary goal is to demonstrate the value of combining first-principles theory and EXAFS to study structurally complicated materials. The results of first-principles theory are of value to the EXAFS experimentalist by guiding the analysis of the structurally complex material. In turn, EXAFS results are of value to the first-principles theorist by measuring the true local structure, without the approximations involved in electronic structure calculations.

Equation (1) has an infinite number of terms. Such an expansion is useful in practice if only a finite, and preferably small, number of the couplings are non-negligible. In Sec. I, we use physical arguments to truncate Eq. (1) to a small number of terms, yielding a model for the local structure. We then show how first-principles calculations can be used to determine the parameters for a given truncation and estimate how well the model captures the local distortions. In Sec. II we present the details of our EXAFS measurements on $Pb_{1-x}Ge_xTe$. In Sec. III we use the model suggested by the first-principles calculations to analyze our EXAFS data. Finally in Sec. IV we summarize the use of both first-principles and EXAFS methods in describing the local structure in $Pb_{1-x}Ge_xTe$.

I. FIRST PRINCIPLES THEORY OF $Pb_{1-x}Ge_xTe$

Bonding considerations in $Pb_{1-x}Ge_xTe$ help to reduce the full cluster expansion of the ionic positions at low temperature given in Eq. (1) to a form that is more tractable theoretically and experimentally. The bonding in $Pb_{1-x}Ge_xTe$ is largely the covalent bonding of p orbitals of Pb, Ge, and Te.[2] However, there is only one valence electron per bond. There is thus a tendency in each linear segment of three ions for the central ion to prefer an off-center position, forming a short bond on one side into which the electron from the long bond on the other side is partially transferred.[2,3] Since both the equilibrium bond lengths and local charge transfer are cation dependent, substitution of one cation species for another should most strongly affect the collinear Te coordinate of the neighboring Te ions and the collinear coordinates of the cations beyond the neighboring Te ions as charge is transferred to or from the central bonds. In terms of Eq. (1), we truncate to linear order and include only those cation neighbors expected to strongly influence the ionic position. For Te ions, only the terms for first-neighbor cations at distance $a/2$ are kept. For Pb and Ge, only the terms for the cations at distance a are kept. Finally, for each Cartesian component of ionic motion, only terms involving the neighbors in the corresponding direction are kept.

TABLE I. Local configurations and displacements from nominal positions eight-term model for $Pb_{1-x}Ge_xTe$. The configurations are the four possible arrangements of ions along any Cartesian directions for each of the three central atoms. The displacements of the ions are given in terms of the parameters in Table II. The net vector displacement of each ion is the superposition of the displacements due to the linear configurations in each Cartesian direction.

Pb configuration	Displacement
Pb–Te–Pb–Te–Pb	0
Pb–Te–Pb–Te–Ge	P_R
Ge–Te–Pb–Te–Pb	P_L
Ge–Te–Pb–Te–Ge	P_L+P_R
Ge configuration	**Displacement**
Pb–Te–Ge–Te–Pb	G_0
Pb–Te–Ge–Te–Ge	G_0+G_R
Ge–Te–Ge–Te–Pb	G_0+G_L
Ge–Te–Ge–Te–Ge	$G_0+G_L+G_R$
Te configuration	**Displacement**
Pb–Te–Pb	T_0
Pb–Te–Ge	T_0+T_R
Ge–Te–Pb	T_0+T_L
Ge–Te–Ge	$T_0+T_L+T_R$

Because $Pb_{1-x}Ge_xTe$ has rhombohedral symmetry at low temperatures, some of the parameters in Eq. (1) are related by symmetry. Our orientation convention for polarization defines [111] as the rhombohedral axis; thus, for Cartesian coordinates α and β,

$$u_{S,\alpha}=u_{S,\beta},$$

$$J_{S,\alpha,d\hat{\alpha}}=J_{S,\beta,d\hat{\beta}}.$$

Nine independent terms remain: $u_{\mathrm{Pb},x}$, $u_{\mathrm{Ge},x}$, $u_{\mathrm{Te},x}$, $J_{\mathrm{Pb},x,a\hat{x}}$, $J_{\mathrm{Pb},x,-a\hat{x}}$, $J_{\mathrm{Ge},x,a\hat{x}}$, $J_{\mathrm{Ge},x,-a\hat{x}}$, $J_{\mathrm{Te},x,a\hat{x}/2}$, and $J_{\mathrm{Te},x,-a\hat{x}/2}$. For simplicity of notation, we rename these terms $u_{\mathrm{Ge},x}\equiv G_0$, $J_{\mathrm{Ge},x,a\hat{x}}\equiv G_R$, $J_{\mathrm{Ge},x,-a\hat{x}}\equiv G_L$, etc., where 0 indicates the coordinate in the case of neighboring Pb cations and L (R) indicates the effect of replacing the left (right) Pb neighbor by Ge. By virtue of translational symmetry, P_0, G_0, and T_0 are not independent; we set $P_0=0$ to obtain a model with eight parameters. We call this the ''eight-term model.'' The effect of these eight parameters on the possible linear chains of Pb, Ge, and Te atoms is shown in Table I.

Further approximations are possible. In pure PbTe, the ground state has the rocksalt structure. If one assumes that Pb ions in the solid solution remain in their rocksalt positions as they do in pure PbTe, and likewise that Te maintains its rocksalt coordinate in a given direction when the corresponding neighbors in that direction are both Pb, then $P_L=0$, $P_R=0$, and $T_0=0$. We call this simpler model the ''five-term model'' and use the expressions in Table I with those three parameters set to 0.

For any given truncation in the cluster expansion, theoretical values for the parameters can be found by fitting a sufficient set of structures to the model. Cockayne and Rabe have made local-density-functional theory studies [4–6] of sev-

TABLE II. Theoretical distortion parameters in $Pb_{1-x}Ge_xTe$ for various models. All values for the linear distortion parameters in the upper panel are given in Å. In the lower panel, the root-mean-square errors of the least-squares fits to density-functional relaxations of three ordered supercells shown in Ref. 4 are given in Å. The root-mean-square errors are given for fits in three dimensions to the set of all ions in the crystal and for each individual species.

Model	Eight-term	Five-term	Islam and Bunker	Null
P_L	0.030	0	0	0
P_R	0.030	0	0	0
G_0	0.060	0.060	0.089	0
G_L	0.057	0.057	0	0
G_R	0.057	0.057	0	0
T_0	−0.029	0	0	0
T_L	−0.164	−0.187	0	0
T_R	0.098	0.074	0	0
$\Delta\mathbf{u}_{rms}$	0.036	0.052	0.126	0.137
$\Delta\mathbf{u}_{rms}$(Pb)	0.024	0.048	0.048	0.048
$\Delta\mathbf{u}_{rms}$(Ge)	0.024	0.024	0.065	0.167
$\Delta\mathbf{u}_{rms}$(Te)	0.044	0.059	0.170	0.170

eral ordered supercells of $Pb_{1-x}Ge_xTe$ at $x=0.25$ in order to study the effect of the local environment on structural, ferroelectric, and piezoelectric properties. The calculations were performed using pseudopotentials, a plane-wave basis set for the electronic wave functions, and conjugate gradients minimization of the total energy. For each of three eight-atom supercells (cells cP8, tP8, and tI16 in Fig. 1 of Ref. 4), a full relaxation of ionic and cell parameters was performed, after biasing the initial ionic positions by displacing the Ge ions 0.25 Å in the [111] direction.[4–6] The distortions of the relaxed cells from pseudocubic were small. We thus assume (pseudo)cubic cells for all subsequent analysis. The origin of each cell was chosen so that P_0 was 0. After weighting the results for each local environment by their relative frequencies in disordered $Pb_{1-x}Ge_xTe$, a least-squares fit of the set of all ionic displacements from the nominal ionic positions was done for four models: the eight-term and five-term models described above, the Islam and Bunker[1] model, in which all of the Ge ions are displaced the same amount along the [111] direction, and the ''null'' model, where the ideal rocksalt structure was assumed. The results are shown in Table II.

Table II shows how well the various models describe the theoretical local distortion in $Pb_{0.75}Ge_{0.25}Te$ supercells, as well as showing the dominant physics affecting this distortion. In the ''null'' model, where the ideal rocksalt structure is assumed, the rms error in atomic positions is 0.137 Å. The rms error for the Ge ions is 0.167 Å, supporting the Ge off-centering picture. The simplest model that captures Ge off-centering is the Islam and Bunker model, where all Ge ions are displaced the same amount from their nominal ionic positions in the cubic [111] directions. In this model, the theoretical rms error for the Ge positions is reduced by more than 60%. However, the overall rms error only goes from 0.137 Å to 0.126 Å. It is necessary to include additional distortions in order to improve upon the Islam and Bunker model. In fact, the theoretical rms Te displacement is as large as that for Ge. The individual parameters with the largest magnitude in the eight-term model are T_L and T_R. Physically, this corresponds to local relaxation. Te relaxes toward the neighboring Ge ion whenever there is a linear Ge-Te-Pb segment. This relaxation is due to the small ionic radius of the Ge ion compared to the Pb ion. When the Ge ion is to the left (right) of the Te, relaxation is toward the left (right) as indicated by the negative (positive) value of T_L (T_R). The asymmetry between T_R and T_L shows that in addition to relaxation, Te ions have a small but important ''recoil'' in the opposite direction to Ge displacement. This is a manifestation of typical ferroelectric distortion where cations are displaced from centrosymmetric positions in one direction and anions in the opposite direction. Including the Te parameters greatly reduces the rms error of the model. Another important secondary distortion arises from the G_L and G_R terms. With these terms in the model, the Ge ions are no longer all displaced off-center by the same amount. The positive values of these parameters can be explained by the coupling of Ge off-centering to Te relaxation. When the cation neighbors of a given Ge ion beyond the Te neighbors are Pb, the Te neighbors relax toward the Ge. This suppresses the tendency of the Ge to move off-center due to the additional short-range Ge-Te repulsion. The set of ordered supercells studied does not allow G_L and G_R (or P_L and P_R) to be determined independently, thus we set them to the same value in Table II. Finally, the differences between the five-term and eight-term models are relatively small. The five-term model contains the five terms of greatest magnitude from the eight-term model, justifying the approximations made. In particular, the results in Table II suggest that the local Pb distortion is small and not crucial to obtaining a good description for the local structure of $Pb_{1-x}Ge_xTe$. The eight-term model still has a 0.036 Å rms error for the ionic positions. In order to improve upon this model, higher-order and/or longer-range terms of Eq. (1) must be included.

In Secs. III B and III C, we present a detailed EXAFS study of $Pb_{1-x}Ge_xTe$ with $x\approx0.3$ based on the five-term model.

II. EXPERIMENTAL DETAILS

Our $Pb_{1-x}Ge_xTe$ sample was prepared by solid solution of stoichiometric ratios of high purity, metallic Pb, Ge, and Te at 1225 K followed by over 360 h of annealing at 825 K. The sintered pellets of $Pb_{1-x}Ge_xTe$ with $x\approx0.3$ were ground with mortar and pestle and sieved to a size appropriate for our EXAFS measurements. The powdered material had a lattice constant of 6.339(1) Å as determined by x-ray diffraction at room temperature. This lattice constant is consistent with $x=0.27(1)$.[7]

Samples were prepared for measurement in the transmission EXAFS geometry[8] for each of the three edges. For each sample, the material was uniformly dispersed within a quantity of graphite and cold pressed into a pellet for easy handling. The samples for the Pb L_{III} and Te K edges had edge steps of ~1, while the Ge K edge sample had a step of $\sim\frac{1}{4}$. The powders were sieved such that the average particle size in the measured sample was small compared to the absorption length. Preparing samples in this manner helps minimize distortions to the data due to sample nonuniformity[9] and particle size effects.[10]

The Te K edge EXAFS data were collected at the National Synchrotron Light Source at beamlines X11a and the Pb L_{III} and Ge K edge data were collected at X23a2. Both of these beamlines use bending magnets to generate photons, which are used unfocused and monochromated by two-crystal 311 silicon monochromators. For all measurements, the vertical dimension of the beam incident upon the sample was defined by slits to be as large as possible without loss of experimental resolution due to beam divergence. For these measurements, the samples were mounted on the cold finger of a Displex cryostat and data were collected at 40, 100, 150, and 200 K. These temperatures are all well below the ferroelectric to paraelectric phase transition temperature of ~ 350 K.[7]

III. DATA ANALYSIS

A. Data processing

Four or more scans were collected at each temperature and each edge. Each scan was normalized using a standard algorithm[11] of pre-edge subtraction and edge-step normalization. Example spectra for each edge are shown in Fig. 2. The normalized spectra from each edge at the various temperatures are then aligned in energy.

The fine structure oscillations are isolated using the AUTOBK (Ref. 12) program. The background function is approximated using a spline with knots evenly spaced in photoelectron wave number. The values of the spline at the knot energies are found by optimizing $\tilde{\chi}(R)$, the Fourier transform of the isolated $\chi(k)$ spectrum. $\tilde{\chi}(R)$ is obtained by isolating $\chi(E)$ according to

$$\chi(E)=\frac{\mu(E)-\mu_0(E)}{\Delta\mu}, \tag{2}$$

where $\mu_0(E)$ is the background spline and $\Delta\mu$ is the edge step, which was set to 1 during the normalization step of the data processing. The abscissa is converted from energy to photoelectron wave number k by the relation $k=\hbar^{-1}\sqrt{2m(E-E_0)}$. $\chi(k)$ is then Fourier transformed over a specified k range to produce $\tilde{\chi}(R)$. The spline is adjusted so that this experimentally derived $\tilde{\chi}(R)$ best matches the $\tilde{\chi}(R)$ obtained from a theoretical calculation using the FEFF6 (Ref. 13) program. The parameters used to determine the background splines are given in Table III and the splines are shown in Fig. 2. The $\chi(k)$ functions extracted from the $\mu(E)$ using AUTOBK are shown in Fig. 3.

The parameter R_{bkg} in Table III determines the number of spline knots used to approximate the background function $\mu_0(E)$. The EXAFS measurement is treated at this stage as a bandpass limited signal, thus the number of knots is determined by the Nyquist criterion.[14] The bandwidth of the signal is determined by the k range of the background removal shown in Table III and by the R range between 0 and R_{bkg}. Thus we presume that the signal below R_{bkg} is dominated by the Fourier components of $\mu_0(E)$ and has negligible local structural content. As discussed in Sec. III B, the FEFFIT (Ref. 15) program is used to analyze the $\chi(k)$ data. FEFFIT allows the user to refine the background spline along with the structural parameters when analyzing the $\chi(k)$ data. This allows evaluation of the correlations between the background spline and the structural fitting parameters. The value of R_{bkg} is chosen to provide the maximum number of spline knots without introducing significant correlation between the val-

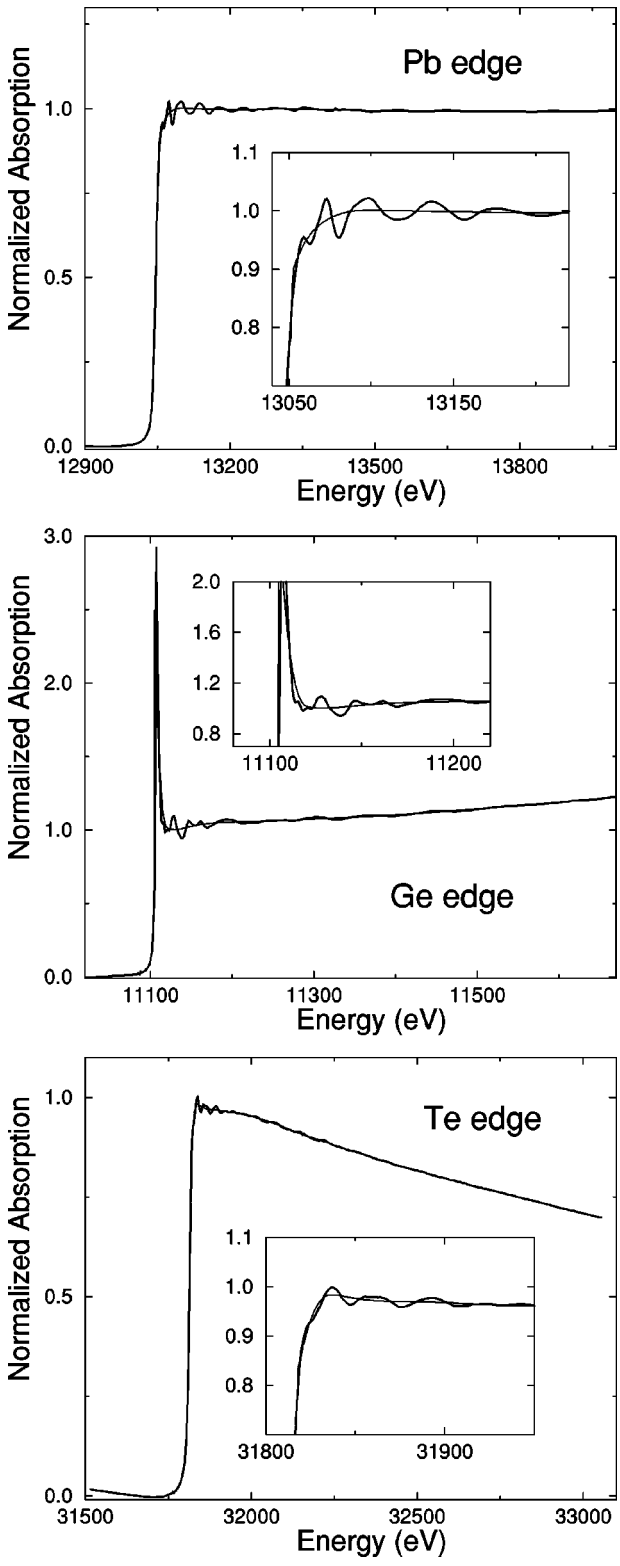

FIG. 2. $\mu(E)$ data (thick lines) at the Pb L_{III}, Ge K, and Te K edges at 100 K. The insets show detail of the regions near the edges. The background functions (thin lines) were determined using the AUTOBK program (Ref. 12) and the parameters in Table III.

TABLE III. Background removal parameters used in AUTOBK. The k range is the range over which a spline using N_{knots} knots was optimized to approximate the background function. The number of knots is determined by $2R_{bkg}\Delta k/\pi+1$.

Element	k range (Å^{-1})	R_{bkg} (Å)	N_{knots}
Pb	[1.00:16.10]	1.5	15
Ge	[1.25:12.45]	1.7	13
Te	[1.00:15.05]	2.0	19

ues of the spline parameters and the structural parameters measured in the fit.

B. Using first-principles theory to guide the fitting model

The first-principles theory indicates that the local structure in $Pb_{1-x}Ge_xTe$ is highly disordered due, in large part, to the extreme size mismatch of the Pb and Ge anions. From the earlier work of Islam and Bunker[1] on $Pb_{1-x}Ge_xTe$, we know that the distribution of Te atoms in the first coordination shell about the Ge anion is split into peaks separated by a large fraction of an angstrom. The presence of the various secondary distortions discussed in Sec. I further adds to the disorder in the pair distribution functions.

A common approach to the analysis of EXAFS data involves modeling pair distribution functions in terms of a cumulant expansion. This approach is not promising for a material as disordered as $Pb_{1-x}Ge_xTe$. Modeling highly disordered, split-peak pair distribution functions would require an inordinate number of cumulant terms. Consequently we sought a way of representing the pair distribution functions in a manner which would more directly measure the distortions to the structure, which could be directly compared with the first-principles theory, and which could be expressed in a small number of variable parameters.

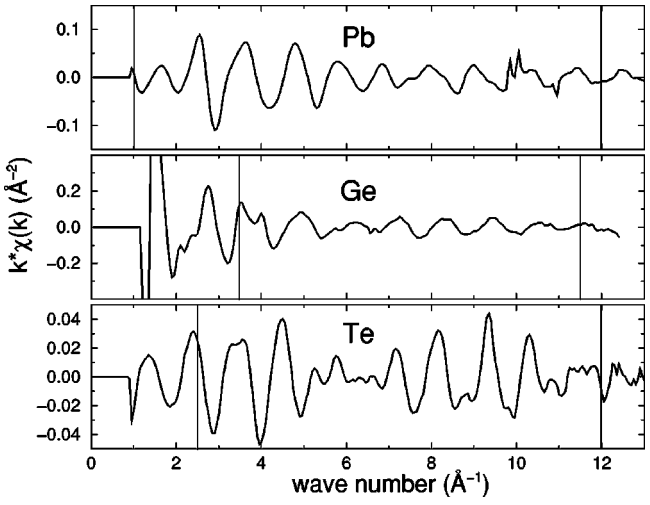

FIG. 3. $\chi(k)$ at 40 K as extracted from the $\mu(E)$ of the three edges shown in Fig. 2 using the AUTOBK program (Ref. 12). Each spectrum is the average of four or more measurements. Each $\chi(k)$ function is multiplied by k to emphasize the high-energy oscillations. The vertical lines indicate the k ranges over which the data were then Fourier transformed and analyzed. Deviations between successive scans are of similar size to the width of the lines, so error bars are omitted in this figure.

By iterating over all linear configurations described in Table I and over all three spatial directions, the pair distribution functions about each central atom can be described as a set of histograms. Each bin in each histogram represents a single-scattering geometry characterized by an atomic species found at some radial distance away from a central atom. The height of the each bin represents the probability of finding an atom at that distance. That height is determined only from the symmetry of the rocksalt structure and the doping fraction as the Pb and Ge ions are assumed to be completely substitutionally disordered. Since the doping fraction is a known quantity, the heights of the bins are fixed values in the fits to the data. The location in radial distance of each bin is determined by the values of the lattice constant and of the distortion parameters from Table II. The pseudocubic lattice constant is a known quantity, thus all of the radial distances to all of the backscatterers considered in the fitting problem are determined by fitting the five distortion parameters. In this way, very complicated radial distributions are modeled using only five structural parameters.

The radial distance to each bin j in the histograms is determined by considering the effects of the distortion parameters to second order. For bin distances R_j out to the third coordination shell, we find a set of polynomials describing the distances R_j of the form

$$\begin{aligned}\frac{R_j^2}{a^2} = N &+ \gamma^j_{G_0}G_0 + \gamma^j_{G_L}G_L + \gamma^j_{G_R}G_R + \gamma^j_{T_L}T_L + \gamma^j_{T_R}T_R \\ &+ \gamma^j_{G_{00}}G_0^2 + \gamma^j_{G_{LL}}G_L^2 + \gamma^j_{G_{RR}}G_R^2 + \gamma^j_{T_{LL}}T_L^2 + \gamma^j_{G_{RR}}G_R^2 \\ &+ \gamma^j_{G_0G_L}G_0G_L + \gamma^j_{G_0G_R}G_0G_R + \gamma^j_{G_0T_L}G_0T_L \\ &+ \gamma^j_{G_0G_R}G_0T_R + \gamma^j_{G_LG_R}G_LG_R + \gamma^j_{G_LT_L}G_LT_L \\ &+ \gamma^j_{G_LT_R}G_LT_R + \gamma^j_{G_RT_L}G_RT_L + \gamma^j_{G_RT_R}G_RT_R \\ &+ \gamma^j_{T_LT_R}T_LT_R\,. \end{aligned} \tag{3}$$

$N \in \{1,2,3,4\}$ is the index of the coordination shell and a is the pseudocubic lattice constant. The γ^j are the coefficients of the distortion parameters. These are always integers as they are determined by the combinatorics of superposing the linear configurations in three dimensions. Each polynomial has associated with it a probability of occurrence dependent upon the crystal symmetry and the doping fraction, as stated above. Summing the probabilities of all possible scattering geometries (i.e., bins) in a shell yields the coordination of that shell.

Considering single-scattering paths out to the third coordination shell about Pb and Te and the second coordination shell about Ge generates over 1000 bins with a precision in distance of 10^{-3} Å. Although tractable, this is a rather large number. Simply ignoring the second-order terms in Eq. (3) significantly reduces the number of bins, but it also introduces a large systematic error to the determination of distances. Although the second-order terms are small, their net contribution to the distortion model is to increase the distances between atoms. Thus neglecting the second-order

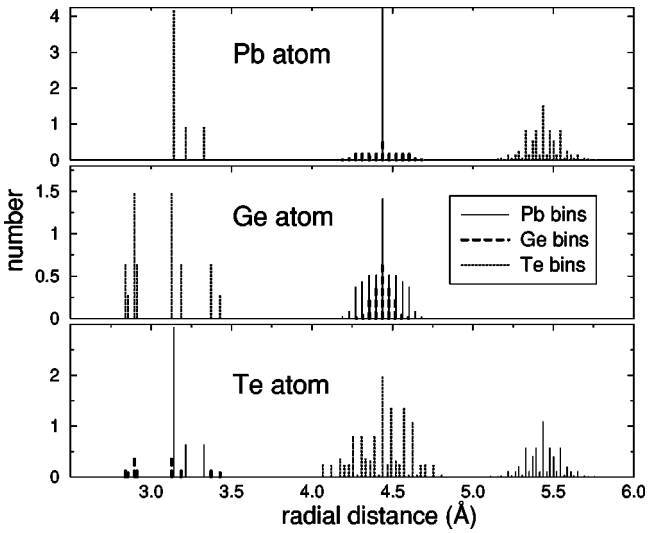

FIG. 4. The set of histograms given by Eq. (3) and the predicted values for the distortion parameters from Table II. These are the histogram bins actually used in the fits to the EXAFS data and include two coordination shells around the Ge atom and three coordination shells around the Pb and Te atoms, although the third-shell Ge atoms are not included in the fits. Note that, since the lead sublattice is undistorted in the five-term model, the second-shell Pb–Pb forms a single bin which is taller than the top panel.

terms biases all distances to smaller values, thus introducing a systematic error to the measurement of the distortion parameters.

Rather than explicitly considering all second-order terms or simply neglecting them, we approximate their effect in a manner that reduces the number of bins in the histograms. To do this, we treat all the first-order terms in Eq. (3) exactly and statistically average the effect of the second-order terms by their probabilities of occurrence. This reduces the number of bins to 201 while also greatly reducing the size of the systematic error caused by simply neglecting those terms. The polynomials using the averaged second-order terms are of the same form as Eq. (3), but the second-order coefficients are replaced by noninteger, effective coefficients $\overline{\gamma^j}$. Using the predicted values for the distortions parameters given in Table II in Eq. (3) yields the set of histograms shown in Fig. 4.

In FEFFIT, the fitting model is expressed as a sum over all scattering geometries j. Each individual scattering geometry (also called a path) is described by an appropriate theoretical fitting standard from FEFF. The fitting standards are modified according the EXAFS equation[8]

$$\chi_F(k) = \mathrm{Im}\sum_j \frac{N_j S_0^2 F_j(k)}{2kR_j^2} e^{i[2kR_j+\Phi_j(k)]} e^{-(2k^2\sigma_j^2)}. \quad (4)$$

This equation expresses the total calculated $\chi_F(k)$ for a particular central atom as a sum over all scattering geometries about that atom. The effective scattering amplitudes $F_j(k)$ and phase shifts $\Phi_j(k)$ for each path are calculated[16] using FEFF. For each path j, FEFFIT can modify the path distance R_j, the mean-square displacement σ_j^2 about R_j, and the amplitude $N_j S_0^2$ in some manner specified by the fitting model. In our case, the R_j of each path is calculated according to Eq. (3), N_j is set to the probability of occurrence of the path, and the passive electron reduction factor S_0^2 is a variable in the fit. Each bin in Fig. 4 represents a term in the summation. All paths are summed together and the sum is fitted to the measured $\chi(k)$ by varying the five distortion parameters along with various other fitting parameters. The fitting is made using a Levenberg-Marquardt algorithm. FEFFIT also allows a shift E_0 in the energy reference for each path which modifies the effective photoelectron wave number by the relation $k = [2m(E-E_0)]^{1/2}/\hbar^2$. All parameters used in the fits are explained in Table IV.

Because we measured data at all three edges, we are able to analyze these data together at each temperature. As the distortion parameters effect the radial distribution functions about all three central atoms, simultaneously refining these data sets provides a robust measurement of those parameters. The program FEFFIT (Ref. 15) is used for the analysis presented in this section. FEFFIT allows fitting of multiple data sets and the construction of the complicated fitting model which uses Eq. (3) to express the path distances.

By fitting the three data sets simultaneously we not only obtain a better measure of the five distortion parameters than if we had fit the data sets independently, we also significantly reduce the number of variables that must be determined in our fits, thus improving the statistical significance of the results. For example, the σ^2 for a given interatomic distance is the same regardless of which atom is the central atom. Therefore, the number of σ^2 parameters varied in the fits is reduced almost by a factor of 2 compared to the number of these parameters needed to fit the data from each edge separately.

The use of five energy shift parameters in these fits merits discussion. To obtain physically reasonable results for certain fitting parameters, it may be necessary to correct errors in the calculation of the central and backscattering phase shifts by FEFF. This may be done by adding an energy shift for each atomic species.[17] A naive application of this phase correction scheme would result in the use of nine energy parameters, i.e., one for each of the three species in each of the three data sets. We found that the use of nine independent energy parameters yielded no statistical improvement over the energy correction model actually used in the analysis reported in this paper. Each data set certainly requires one overall energy correction to align the data with the fitting standard. This overall correction is applied to the Te backscatterer at each edge. Since the potentials and phase shifts of the fitting standards are calculated in similar manner[18] for each absorber, we assume that the differences in the energy corrections required for the Pb and Te atoms are the same for each central atom. Thus the Pb backscatterers are energy corrected by the sum of the overall correction and a difference parameter $\Delta E_0(\mathrm{Pb})$. That parametrization of the Pb phase correction is used for all three edges. Similarly, the Ge backscatterers are energy corrected using a parameter $\Delta E_0(\mathrm{Ge})$. This reduces the number of energy correction parameters almost in half, from 9 to 5.

In total, we used 19 fitting parameters to fit the data from the three edges at each temperature. In any fitting algorithm, it is essential not to overspecify the problem by attempting to fit more parameters than are allowed by the available data. A common method of estimating the available information in

TABLE IV. A summary of the fitting parameters used in the fits to the three edges. In total, 19 parameters are determined from the three data sets at each temperature. The parameters marked with a star (⋆) are analyzed for their temperature dependence. The parameters marked with a dagger (†) affect data from more than one edge. For the S_0^2 and energy shift values the best-fit values are averages over temperature. The results for the distortion parameters are shown in Fig. 6. For the mean-square displacements, the Einstein temperature corresponding to the temperature dependence of the parameter is reported. The Einstein temperatures for the second-shell paths containing Ge are not given, as explained in the text.

	Parameter	Description	Best-fit value
	S_0^2(Pb)	Passive electron reduction factor for the Pb atom	0.83(3)
	S_0^2(Ge)	Passive electron reduction factor for the Ge atom	0.87(8)
	S_0^2(Te)	Passive electron reduction factor for the Te atom	1.10(6)
⋆†	G_0	Ge off-center displacement	See Fig. 6
⋆†	G_L	Additional Ge displacement due to a Ge on the left	See Fig. 6
⋆†	G_R	Additional Ge displacement due to a Ge on the right	$\equiv G_L$
⋆†	T_L	Te displacement due to a Ge on the left	See Fig. 6
⋆†	T_R	Te displacement due to a Ge on the right	See Fig. 6
	$E_{0,\mathrm{Te}}$(Pb)	Energy shift of the Te backscatterer at the Pb L_{III} edge	−3.14(14)eV
	$E_{0,\mathrm{Te}}$(Ge)	Energy shift of the Te backscatterer at the Ge K edge	−3.90(1.52) eV
	$E_{0,\mathrm{Te}}$(Te)	Energy shift of the Te backscatterer at the Te K edge	2.58(42) eV
†	ΔE_0(Pb)	Energy shift of the Pb backscatterer relative to the Te for each edge	−0.63(56) eV
†	ΔE_0(Ge)	Energy shift of the Ge backscatterer relative to the Te for each edge	4.67(1.03) eV
⋆†	σ^2(Pb,Te)	Mean-square displacement between Pb and Te, 1st shell	122(9) K
⋆†	σ^2(Ge,Te)	Mean-square displacement between Ge and Te, 1st shell	225(80) K
⋆	σ^2(Pb,Pb)	Mean-square displacement between Pb and Pb, 2nd shell	57(3) K
⋆	σ^2(Ge,Ge)	Mean-square displacement between Ge and Ge, 2nd shell	
⋆	σ^2(Te,Te)	Mean-square displacement between Te and Te, 2nd shell	112(14) K
⋆†	σ^2(Pb,Ge)	Mean-square displacement between Pb and Ge, 2nd shell	
⋆†	σ^2(Pb,Te)	Mean-square displacement between Pb and Te, 3rd shell	71(23) K

an EXAFS measurement is to treat the data as a bandpass limited signal and so to use the Nyquist criterion.[14,19] Thus the available information is related to the product of the width in k space of the Fourier transform window applied to the $\chi(k)$ data and the width in R space over which the data is fit. There is some ambiguity as to how the Nyquist criterion should be applied to a multiple data set fit. Assuming the information content of the three data sets is the sum of their bandwidths, there are about 57 independent measurements in our data at each temperature. A recent Bayesian treatment of EXAFS data[20] demonstrates that the information content of the data is typically less than that predicted by the Nyquist criterion by $\frac{2}{3}$ or more. Even so, it is reasonable to expect that we can measure 19 well chosen parameters. This is confirmed by our ability to measure physically reasonable values with small uncertainties for our parameter set.

C. Results of the fits

An example of a fit obtained using the fitting model described in Sec. III B and fitting the three edges concurrently is shown in Fig. 5 for the data at 100 K. We obtain excellent fits for all three edges. Repeating this analysis for the temperature range 40–200 K, we can measure the temperature dependence of the fitting parameters. As indicated in Table IV, the E_0 and S_0^2 parameters should be temperature independent. Indeed, these parameters are constant in temperature within the indicated error bars and are found to be of physically reasonable values, with the single exception of the the S_0^2 value for the Te K edge. The energy shift parameters are small corrections to calculation errors in the fitting standards. The S_0^2 values for Pb and Ge are in agreement with the theoretical values of 0.84 and 0.83, respectively, as calculated by FEFF. The S_0^2 value for Te exceeds 1, which is not physically reasonable. The cause of this unreasonable result will be addressed below in the discussion of the σ^2 parameters.

The temperature dependences of the measured distortion parameters are shown in Fig. 6. In Sec. I, we state that the supercells used in the LDFT cannot independently determine the parameters G_L and G_R. This was true of our analysis also. When varied independently, these parameters were equal within their error bars and varying them independently did not result in a statistical improvement improvement to the fit. Thus we just show G_L in Fig. 6. Recall that these parameters describe atomic displacements along each Cartesian direction. Also shown in Fig. 6 is the temperature dependence of the off-center displacement in three dimensions of the Ge atom as computed from structural parameters.

Figure 6 shows the temperature dependence of the structural parameters along with their values predicted by first-principles theory. The theory predicts that G_0, G_L, and T_R are of roughly the same size in the five-term model. This is true of our measurements as well, although at low temperatures these terms are larger than predicted by about a factor of 2. This trend may be explained in part by the use of the local-density approximation (LDA) in the first-principles calculations. The LDA predicts a pseudocubic lattice parameter for $Pb_{1-x}Ge_xTe$ that is smaller than the crystallographically determined one.[7] The first-principles calculations show that

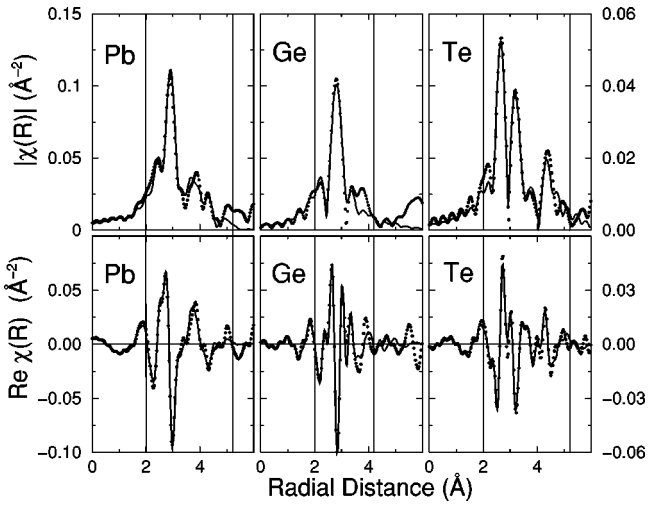

FIG. 5. Results of the corefinement of the Ge and Te K edges and the Pb L_{III} edge EXAFS at 100 K. The data are shown as points and the best fits as lines. The upper sequence of panels show the magnitude of the complex Fourier transform of $\chi(k)$ and the bottom sequence shows the real part. The vertical lines indicate the fitting ranges. The scale of the Pb and Ge data is shown on the left and the scale of the Te data is shown on the right.

the structural parameters are positively correlated to the size of the unit cell. It is thus unsurprising that the first-principles predictions for these parameters are smaller than the values measured by EXAFS. It is also possible that the local structures in the high-symmetry ordered supercells that we studied are unrepresentative of those in the disordered experimental system. Including additional supercell calculations and carefully accounting for strain effects[21] due to the size mismatch of Pb and Ge should lead to a theoretical model

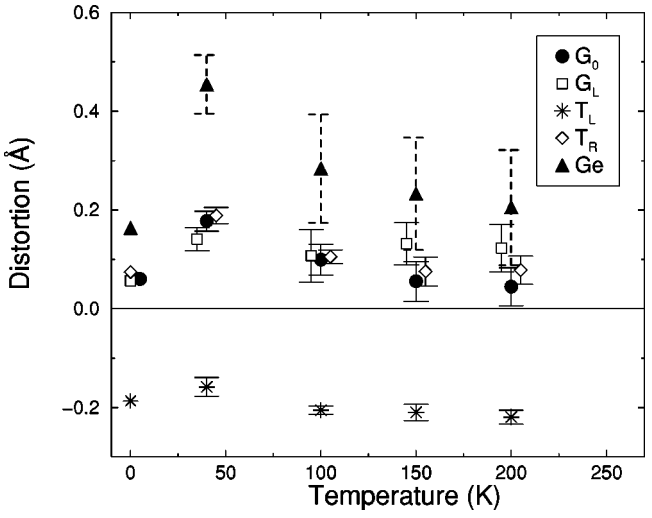

FIG. 6. Temperature dependence of the distortion parameters. These parameters are described in Table IV. G_0 is the solid circles (●), G_L is the squares (□), T_L is the asterisks (*), and T_R is the diamonds (◇). For clarity, the squares and diamonds are displaced to the left and right. The triangles (▲) represent the displacement in three dimensions of the Ge atom from its nominal lattice position averaged over the possible local environments in the $x \approx 0.3$ material. The points at 0 K represent the theoretical predictions for these values from Table II.

that extrapolates better to disordered configurations. For the above reasons, we believe that the experimental parameters that we obtained describe the local structure in $Pb_{1-x}Ge_xTe$ better than the theoretical ones. The measured value of T_L agrees very well with the predicted value.

The parameters G_0 and T_R show a weak temperature dependence consistent with becoming smaller with increasing temperature. Due to the attenuation of G_0, the displacement of the Ge atom from its nominal lattice position, shown by the triangles (▲) in Fig. 6, also attenuates. Simulations of the local distortions in a model for an ordered cubic Pb_3GeTe_4 supercell at finite temperatures (see Fig. 10 of Ref. 5) show that, below the ferroelectric-paraelectric transition temperature, the anharmonicity in the potential well for the Ge ion tends to lower the mean Ge displacement as temperature increases, in agreement with the experimental results. In contrast, the large T_L parameter shows little temperature variation.

Most of the mean-square displacement parameters σ^2 displayed reasonable temperature dependence. They behave like single frequency oscillators[8] and are well described by an Einstein temperature. The Einstein temperatures[22] describing the temperature dependences of these parameters are reported in Table IV. The small values for the Einstein temperatures are consistent with a structure as open as $Pb_{1-x}Ge_xTe$ and which contains soft bonds between the atoms. We do not report Einstein temperatures for the second-shell paths which include Ge. Because the Ge sublattice is so disordered and because Ge is the minority component, the contribution to the measured signal of second-shell paths containing Ge is very small compared to the other contributions. Although included in the fits, these two mean-square displacement parameters were ill determined in our fits and reliable values for the Einstein temperatures cannot be reported.

By reporting an Einstein temperature, we imply that the behavior of the σ^2 parameters is that of a single-frequency oscillator. In fact, all five of the parameters for which an Einstein temperature is reported deviate from the behavior of a single-frequency oscillator in that, at low temperature, they deviate from the values indicated by the zero-point motions of the bond. At low temperature, four of the σ^2 parameters go to a value that is larger than the zero-point value, while the σ^2 for the Te-Te second-shell paths goes to a much smaller value. This behavior can be understood in terms of the very strong correlation in an EXAFS fit between thermal and structural disorder. Finite temperature and structural disorder both attenuate the $\chi(k)$ signal by a term proportional to k^2. By measuring data at many temperatures, we can determine the thermal portion of the σ^2 parameters as characterized by the Einstein temperature. Any portion of σ^2 in excess of this must be due to mistakes in the structural model used in the fit.

In our measurements, the σ^2 parameters involving Pb atoms are consistently larger than the thermal disorder associated with the Einstein temperatures. This suggests that the structural model used as in the fits contained too little disorder for the lead sublattice. This missing structural disorder was accounted for in the fits by increasing the σ^2's. Similarly, the Te-Te second-shell σ^2 was smaller than the thermal disorder associated with its Einstein temperature. This is

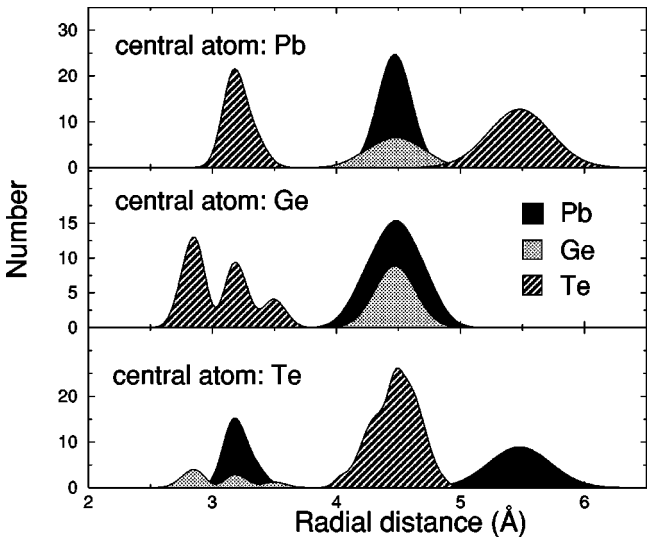

FIG. 7. Radial distribution functions about the three central atoms. These functions are constructed using the histograms determined from the distortion parameters in Table IV broadened by the σ^2 values from the fits at 100 K.

consistent with too much disorder on the Te sublattice in the model. The abnormally large value of S_0^2 for the Te atom is likely due also to the excess Te sublattice disorder. Because σ^2 and S_0^2 tend to be correlated in a fit to EXAFS data, a systematic error in the Te-Te σ^2 is correlated to a systematic error in the determination of S_0^2 for the Te atom.

As explained in Sec. I, we assumed that the Pb sublattice is undistorted and that all of the structural disorder is accommodated by the Ge and Te sublattices. When this assumption is used to fit the distortion parameters to the LDFT structures, we find an excess of entropy in the Ge and Te sublattices and no entropy in the Pb sublattice. Of all the assumptions that entered our structural model, it seems that this is the most severe. This interpretation can be tested by removing the assumption of the undistorted lead sublattice and recasting the fitting model to include parameters describing the displacement of the Pb atom and the couplings of the motions of the Ge and Te atoms to the Pb displacement. This is the topic of Sec. III D.

Using the measured values for the distortion parameters and the measured mean-square displacements, we can construct pair distribution functions for each of the three central atoms. These functions are shown at 100 K in Fig. 7. These pair distributions clearly demonstrate the high degree of disorder in the local structure in this material. In fact, we find that the first Te shell about the Ge central atom is split into *three* peaks and several of the other peaks in the distributions are highly skewed. This supports the assertion made in Sec. III B that the use of cumulants would be inappropriate for this system.

D. Consideration of Pb disorder

As stated above, the lack of disorder in the Pb sublattice is the most serious approximation in the five-term structural model. To address the effect of lead disorder, we now consider the eight-term model of Sec. I. We constrain G_R to be the same as G_L as suggested by the results of Sec. III C. Similarly, we constrain P_R to be the same as P_L, leaving us with a six-term model.

Our six-term model is constructed in the same manner as the previous model. We write polynomials in the manner of Eq. (3) to describe the R_j's of the bins in the histograms. The new polynomials are of the same form as those in Eq. (3), but they have more terms. By considering Pb distortions, we hoped to address the problems in the measured thermal disorder parameters. Unfortunately, this was not the case.

Our fits using the six-term model yielded no improvement in goodness of fit over the earlier fits as measured by a reduced chi-square metric. Furthermore, the new parameter set showed very high correlations between the structural, σ^2, and E_0 parameters.

Because the statistical quality of the fits was not improved, we are forced to reject the six-term model. This is likely not due to a flaw in the model. The six-term model, like the five-term model, is a simplification of the eight-term model which offers a good description of the LDFT structure of $Pb_{1-x}Ge_xTe$. We believe that the six-term model failed by exceeding the measurable information content of the data and by introducing excessive correlations among the parameters.

In the original EXAFS work on $Pb_{1-x}Ge_xTe$, Islam and Bunker considered a structural model which, in the language of this paper, was a one-term model. It only considered the off-center displacement of the Ge atom in the [111] direction. The five-term model used throughout this paper includes Te relaxation, Te ''recoil,'' and the coupling of the Ge displacement to Te relaxation. The six-term model includes Pb disordering and the displacement of the Te ions centered between two Pb ions as well. It is easy to speculate on models which use fewer assumptions and include more parameters. At each stage of complexity, more of the underlying physics of the material is considered. The trick, in this work as in any EXAFS analysis problem, is to determine the level of complexity that can be supported by the available data.

From the LDFT results, there is no obvious cutoff in terms of the magnitudes of the parameters. While the parameters considered in the five-term model are indeed the largest of the eight parameters, the remaining parameters are not much smaller. In general terms, adding more parameters improves the description of the structure at the expense of adding to the scale and complexity of the model and of making the model more prone to statistical instability.

We found a four-term model (i.e., the five-term model with G_L and G_R constrained to be the same) to be the most appropriate in this case. It measures the primary structural features — the off-center displacement of the Ge atom and the relaxation of the Te atom — as well as some secondary distortions and it yields a much more detailed description of the local structure in $Pb_{1-x}Ge_xTe$ than is possible using a simpler model.

IV. DISCUSSION

We have analyzed EXAFS data measured on all three edges of $Pb_{1-x}Ge_xTe$ for the $x \approx 0.27$ alloy and compared this to the results of first-principles calculations on the x

=0.25 alloy. We find significant off-center displacement of the Ge atom, in agreement with earlier EXAFS results.[1] The Ge atom is displaced from its nominal lattice position in a $\langle 111 \rangle$ direction by about 0.25 Å, with increasing displacement as temperature is lowered.

We have significantly extended the earlier results by successfully measuring various secondary distortions in the material. We find that the Te atom relaxes in the presence of the Ge substitution due to the much smaller size of the Ge anion compared to the Pb host and that this relaxation is about the same size as the Ge displacement. We are also able to measure the magnitude of coupling between the Ge displacement and Te relaxation. However, we are unable to determine the amount of disorder on the Pb sublattice. Still, we offer a description of the nature of the local distortions in ferroelectric $Pb_{1-x}Ge_xTe$ which is much more detailed than was previously available.

$Pb_{1-x}Ge_xTe$ possesses a complicated and highly disordered local structure. We wish to highlight several aspects of our analysis that allowed us to successfully resolve details of this structure.

Measurement of multiple edges. We measured data at all available edges in the material and simultaneously refined these data in the fits. Thus we are able to significantly reduce the number of parameters considered in the fits.

Use of a robust fitting model. We base our fitting model on the results of first-principles calculation. We are able to refine fitting parameters which are directly indicative of the essential physics of the material. In $Pb_{1-x}Ge_xTe$, the ferroelectricity is a direct consequence of the local distortions not only of the Ge anion, but of all the atoms in the structure. Our fitting parameters directly measure the interactions between the atoms. Analyzing these data by use of cumulant expansions of the pair distribution functions is not appropriate for such a complex structure.

Use of theoretical fitting standards. Our analysis of $Pb_{1-x}Ge_xTe$ requires the use of theoretical fitting standards. The use of empirical fitting standards is precluded beyond the first coordination shell due to the difficulties of separating higher shells in the standard compounds (presumably PbTe and GeTe). We have no such problem using FEFF. In fact, FEFF allows us to tailor our fitting standards to the needs of the fitting problem.

Using a cluster expansion to describe ground-state structures for arbitrary configurations of a solid solution is exact in principle. By analogy with cluster expansions of total energies for solid solutions,[21] calculations for about 20 supercells are probably sufficient to determine a cluster expansion that contains all of the important physics, even the multibody terms that we have not considered here. The model would then be appropriate for describing any arbitrary configuration, even disordered ones. The parameters in the cluster expansion for a given material lead to a compact and appropriate description of local structure for fitting EXAFS data.

Nonetheless, as we show, EXAFS results are a useful complement to first-principles modeling. EXAFS gives the true local structure, free of the approximations used in first-principles electronic structure calculations. Furthermore, the parameters can be measured directly for a disordered system, as opposed to the theoretical case, where *ab initio* calculations are constrained to relatively small periodic cells. Finally, EXAFS measurements show the temperature dependence of the local structure. First-principles effective Hamiltonians are a tool for investigating the temperature-dependent behavior of complex systems. In the near future, significant progress is likely in developing first-principles effective Hamiltonians for solid solutions. The temperature-dependent description of local structure obtained from EXAFS experiments can provide important constraints and tests for such models.

We find that combining first-principles calculation with EXAFS measurement is a powerful approach to understanding structurally complicated materials. It is well established that the nature of local structural distortions can have profound influence on the macroscopic properties of a wide variety of scientifically and technologically interesting materials, including relaxor ferroelectrics, high dielectric ferroelectric, high-temperature superconductors, and magnetoresistive materials. Many of these advanced materials share with $Pb_{1-x}Ge_xTe$ the feature of being composed of many elements which are suitable EXAFS probes. Consequently, the approach to measurement and analysis employed in this paper is extremely attractive for application to these materials. By measuring EXAFS data at all available edges and fitting the data sets simultaneously using structural models inspired by first-principles results, we predict that highly detailed understandings of the local structures of many advanced materials will be attainable.

ACKNOWLEDGMENTS

We thank B. Bunker for supplying us with a sample, D. Haskel, J. Woicik, and C. E. Bouldin for help collecting data, E. A. Stern for graciously donating beam time, and U. V. Waghmare for guidance in the first-principles calculations. This work was supported in part by the National Research Council and by Office of Naval Research Grant No. N00014-97-J-0047.

[1] Q. Islam and B. Bunker, Phys. Rev. Lett. **59**, 2701 (1987).
[2] P. B. Littlewood, CRC Crit. Rev. Solid State Mater. Sci. **11**, 229 (1984).
[3] G. Lucovsky and R. M. White, Phys. Rev. B **8**, 600 (1973).
[4] E. Cockayne and K. M. Rabe, in *First-Principles Calculations for Ferroelectrics*, edited by R. E. Cohen, AIP Conf. Proc. No. **436** (AIP, New York, 1998), pp. 71–80.
[5] E. Cockayne and K. M. Rabe, Phys. Rev. B **56**, 7947 (1997).
[6] E. Cockayne and K. M. Rabe, Phys. Rev. B **57**, R13 973 (1998).
[7] D. Hohnke, H. Holloway, and S. Kaiser, J. Phys. Chem. Solids **33**, 2053 (1972).
[8] E. A. Stern and S. M. Heald, in *Handbook of Synchrotron Radiation*, edited by E. E. Koch (North-Holland, New York, 1983), Chap. 10, pp. 995–1014.
[9] E. A. Stern and K. Kim, Phys. Rev. B **23**, 3781 (1981).
[10] K. Q. Lu and E. A. Stern, Nucl. Instrum. Methods Phys. Res. **212**,

475 (1983).
[11] D. E. Sayers and B. A. Bunker, in *X-Ray Absorption: Principles, Applications, Techniques of EXAFS, SEXAFS, and XANES*, Vol. 92 of *Chemical Analysis*, edited by D. Koningsberger and R. Prins (John Wiley and Sons, New York, 1988), Chap. 6, pp. 443–571.
[12] M. Newville, P. Līviņš, Y. Yacoby, J. J. Rehr, and E. A. Stern, Phys. Rev. B **47**, 14 126 (1993).
[13] S. I. Zabinsky, J. J. Rehr, A. Ankudinov, R. C. Albers, and M. J. Eller, Phys. Rev. B **52**, 2995 (1995).
[14] L. Brillouin, *Science and Information Theory* (Academic Press, New York, 1962).
[15] E. A. Stern, M. Newville, B. Ravel, Y. Yacoby, and D. Haskel, Physica B **208&209**, 117 (1995).
[16] J. J. Rehr and R. C. Albers, Phys. Rev. B **41**, 8139 (1990).
[17] D. Haskel, B. Ravel, M. Newville, and E. Stern, Physica B **208&209**, 151 (1995).
[18] J. J. Rehr, J. Mustre de Leon, S. I. Zabinsky, and R. C. Albers, J. Am. Chem. Soc. **113**, 5135 (1991).
[19] E. Stern, Phys. Rev. B **48**, 9825 (1993).
[20] H. J. Krappe and H. H. Rossner, J. Synchrotron Radiat. **6**, 302 (1999).
[21] D. B. Laks, L. G. Ferreira, S. Froyen, and A. Zunger, Phys. Rev. B **46**, 12 587 (1992).
[22] E. Sevillano, H. Meuth, and J. Rehr, Phys. Rev. B **20**, 4908 (1979).